

MODELLING AND SIMULATION OF NICKEL SOLUTION PURIFICATION IN INDUSTRIAL JAROSITE AUTOCLAVES

By

Johann Steyl, Suné Grobbelaar, ²Karina Beukes and ²Dirk du Toit

Dynamet Insights (Pty) Ltd, South Africa
²Impala Platinum Ltd - Refineries, South Africa

Presenter and Corresponding Author

Johann Steyl
johann.steyl@dynamet.co.za

ABSTRACT

This paper describes how a hybrid first-principles – machine-learning (FP-ML) modelling and simulation platform can help to understand and improve complex industrial processes. Nickel solution purification, predominantly via ammonium jarosite precipitation in a series of autoclave stages, is presented as a case-study example. The case-study is used to demonstrate the model development workflow and benefits of this transient modelling approach to the industry.

Initial modelling identified info gaps in the operational chemical suite, which prompted a short sampling campaign to measure the key species profiles in the autoclaves. Since precipitation mechanisms are complex and difficult to interpret via batch experimentation, only this sampling campaign data was used. The additional model inputs were the logged plant inflow stream flows and upstream block states.

The workflow methodology is discussed in the paper and only relies on basic chemistry, measurement and understanding. The FP modelling construct is based on acausal mass-energy balance equations (macro model), which take care of the dynamic interactions of each inventory block with its neighbouring blocks. Within this FP framework, phenomenological equations were added and ML algorithms trained to capture the observed chemical behaviour (micro model). The advantage of this approach is that the data-science blocks can deal with the microscopic-scale complexities, while the combined model generalises the behaviour so that it becomes predictive.

The end result is a high-fidelity model that is trained on actual plant data, and which is able to predict actual plant behaviour. Moreover, an implementation platform, with a user-friendly front end, is provided where the model, and the associated benefits, can be made accessible to a wider technical team in the operational environment. This compiled application product (APP) digitally captures the key information and becomes a ‘living report’ of the operation. Validated and predicted trends are presented in the paper, demonstrating that this model qualifies as a true digital twin (DT) that can be used to improve operating strategies and process control, and to help train operators.

Keywords: digital twin, transient modelling, hybrid modelling, simulation, ammonium jarosite, nickel.

INTRODUCTION

Many industrial operations deviate from their design operating points, especially in the case of toll refiners where different feed materials are treated. Furthermore, daily operational challenges often overshadow plant engineers' focus, causing plant sections to underperform metallurgically. Digital twins (DTs) are models that mimic the behaviour of unit blocks in the time domain. As computational power and modelling fidelity improve, DTs will become increasingly important operational and engineering tools to help improve metallurgical performance and process efficiencies. The objective of this paper is to demonstrate the workflow, features and benefits of a hybrid first-principles – machine learning (FP-ML) modelling approach when applied to an actual operating plant.

This case-study focuses on the removal of iron, predominantly as ammonium jarosite, from nickel-rich solutions in an autoclave circuit. Discussing the larger flowsheet configuration is not warranted here since the DT battery limit only covers the two feed tanks – that is, the main feed tank and the weak aqueous ammonia (aqua) tank, and the autoclave vessels (A and B) – see Figure 1. It is however important to note that the main feed tank takes at least three input streams, with varying flows and compositions – these process disturbances are also transferred to the autoclave blocks. Furthermore, weak aqua solution is intermittently dosed via on/off (open/close) valves to the various autoclave compartments, which make the species and chemistry behaviour even more transient. Steady-state (SS) models are incapable of dealing with such complexities. This case-study was therefore the ideal example to demonstrate the hybrid FP-ML transient modelling approach.

A short sampling campaign was undertaken by collecting autoclave profile data to fill some key knowledge gaps. These results are discussed in the paper, emphasising how it helped to close the degrees-of-freedom of the mathematical construct, give confidence in the DT performance during the model validation phase and create insights into the plant operation.

PROCESS MODELLING

Flowsheet

The simplified flowsheet is shown in Figure 1. The logged states refer to the normal plant operation. The feed and aqua tank sections were first modelled so that the simulated results could be reconciled with the logged states. The feed tank states were accurately simulated, as were the feed forward flowrate, composition and temperature to the first autoclave stage (A1). In the case of the aqua tank, the total (integrated) ammonia consumption (over 24 h periods) was logged, as well as the on/off signals of the various aqua valves. The modelled dissolved ammonia concentration approached its saturation point under small positive pressure and slightly elevated temperature variations, varying typically between 22-26 wt% NH_3 . These variations had a relatively small impact on the final DT output and was therefore fixed at an average of 24 wt% NH_3 , which was close to the average aqua concentration measured on the plant over the sampling campaign period.

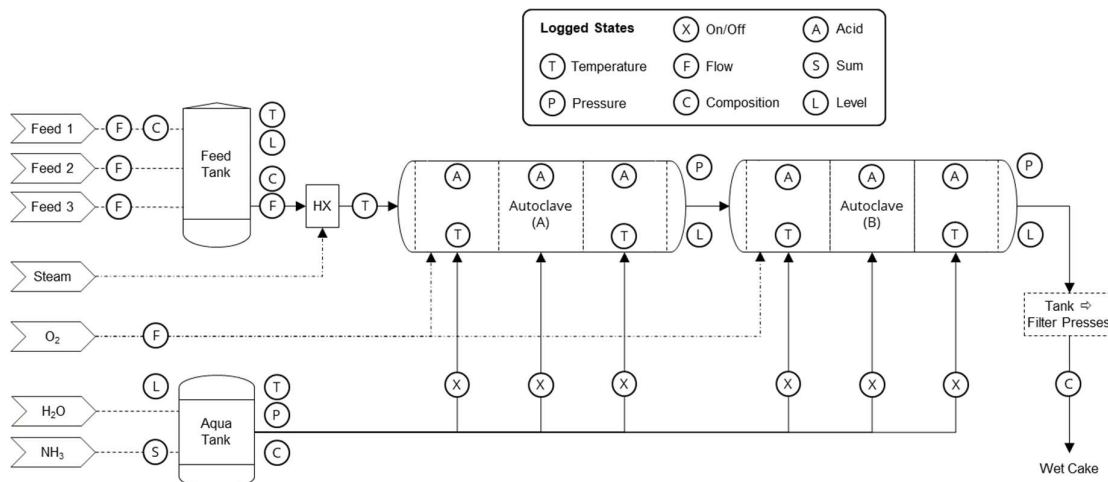


Figure 1: Jarosite Autoclave Section – Simplified Flowsheet.

The weak aqua flow was not measured on the plant and the system had to be constrained by comparing the cumulative ammonia consumption. Figure 2 shows these results for the sampling campaign period, which amounts to an average flow of 15-20 L/min weak aqua per compartment. Since all six on/off valves draw from the same feed pipe, the weak aqua flowrate can vary to any specific compartment when some (or all) of the valves open simultaneously. An additional small flow is also sporadically drawn from the weak aqua tank to a downstream pH adjustment tank, introducing further complexity. Consequently, this is an area where DT model improvement opportunities exist – that is, to measure and record the actual weak aqua mass flows to each compartment on the plant in the future. To simplify the DT model for this initial modelling phase, the flow to each compartment was fixed at an average weak aqua flow of 17.5 L/min.

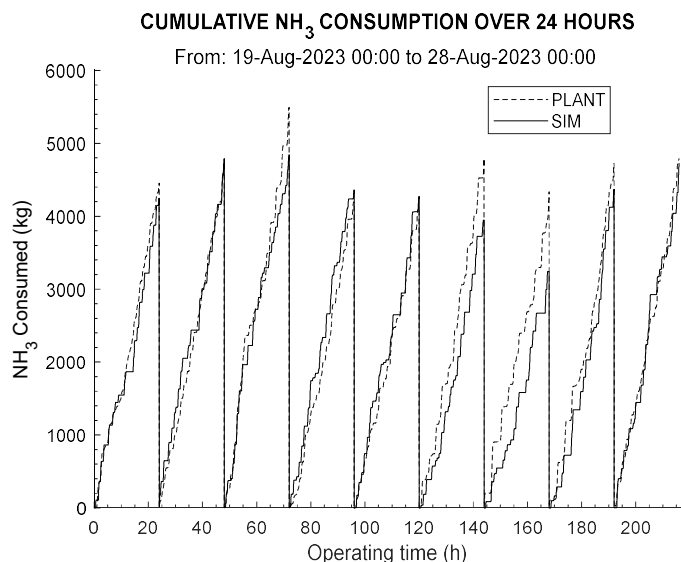


Figure 2: Plant vs simulated ammonia consumption, based on the logged plant on/off signals and an average of 17.5 L/min weak aqua flow to each autoclave compartment.

Macro model

The FP transient mass-energy balance equations of the plant section (Figure 1) represent the macro model. With the feed stream temperatures, flows and compositions accurately mapped, the block states follow directly from the time integration of the system equation set. The detailed DT modelling methodology and FP equation sets have been presented elsewhere⁽¹⁾. The FP equations construct of each flowsheet unit block have been implemented using the MathWorks^{®(2)} Simscape[™] language and a bespoke Metallurgy Domain created by Dynamet⁽³⁾. These algorithms can simultaneously deal with particle-, species- and heat-flow in the time domain, including the system causality. Furthermore, since Simscape is implemented in the Simulink[®] graphical programming environment, the flowsheet model is created by using intuitive drag-and-drop physical-flow connectors between the different unit blocks. Any regulatory and advanced control loops, operating heuristics and event-based aspects, and any derived values, data reconciliations and visualisations are easily dealt with in this single software environment.

Micro model

The micro model describes how the formal species are distributed between the different phases (physico-chemical reactions) and interact chemically with each other (chemical reactions). The first set of equations was used to describe the rapid kinetic changes between the gas species, H₂O_(g), NH_{3(g)}, O_{2(g)}, and their respective liquid-phase states. For example, the oxygen mass-transfer rate, $\dot{m}_{rx,1}$ (kg/s), between the gas and aqueous slurry phase can be described as:

$$\begin{aligned} \text{O}_{2(g)} &\leftrightarrow \text{O}_{2(a)} & 1.1 \\ \dot{m}_{rx,1} &= k_1(m_{y,o_2}^* - m_{y,o_2}) \cdot m_{H_2O} & 1.2 \end{aligned}$$

where k_1 is a lumped parameter that takes care of the physical mixing, temperature variations, and any proportionalities⁽¹⁾. The mass of inventory water in the control volume m_{H_2O} is used to scale the reaction rate $\dot{m}_{rx,1}$ so that the diffusion rate can be expressed as the difference between the

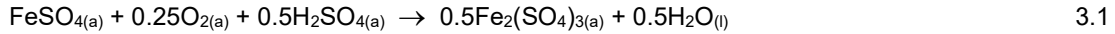
thermodynamic (equilibrium) molality m_{y,O_2}^* (mol/kg), and its current state value. All thermodynamic values in the DT were implemented either as lookup tables from reliable data sources or as ML blocks trained on outputs from state-of-the-art software tools, such as OLI Studio⁽⁴⁾.

Since the iron(II) concentration entering the autoclave is relatively low (< 3 g/L Fe), the interfacial oxygen mass-transfer rate was never rate limiting – there was therefore no need to include k_1 in the ML training routines. On the other hand, with acid neutralisation being an important driver of the various hydrolysis reactions below, it was included (as formal species) via the following reaction:



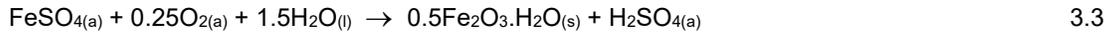
$$\dot{m}_{rx,2} = k_2 = f(m_{\text{H}_2\text{SO}_4}, m_{\text{NH}_3}) \quad 2.2$$

The neutralisation rate k_2 (kg/s) was trained as a function of the formal species block inventory masses, as shown in Equation 2.2. Since weak aqua is sporadically pumped into the various autoclave compartments, the oxidation of iron(II) was simulated via two parallel pathways – the first being the oxidation to the trivalent state in solution:



$$\dot{m}_{rx,3a} = k_3(1 - x_{\text{Fe}}) = f(m_{\text{FeSO}_4}, m_{\text{O}_2}, \dot{m}_{in,\text{FeSO}_4}, \dot{m}_{in,\text{H}_2\text{SO}_4}) \quad 3.2$$

Aside from including the inventory masses, the best training results were obtained by also accounting for the inflow rates \dot{m}_{in} (kg/s) of the indicated species. The fraction of the precipitated iron present as hydrated hematite or goethite phase, $\text{Fe}_2\text{O}_3 \cdot \text{H}_2\text{O}$, is denoted by x_{Fe} , which was assumed to nucleate rapidly in low-acid environment, via the second parallel pathway:



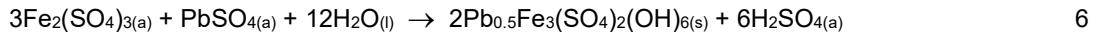
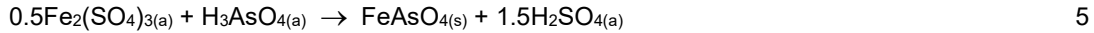
$$\dot{m}_{rx,3b} = k_3 x_{\text{Fe}} = f(m_{\text{FeSO}_4}, m_{\text{O}_2}, \dot{m}_{in,\text{FeS}}, \dot{m}_{in,\text{H}_2\text{SO}_4}, \dot{m}_{in,\text{NH}_3}) \quad 3.4$$

The particle growth mechanism was assigned exclusively to the formation of ammonium jarosite:



$$\dot{m}_{rx,4} = k_4 = f(m_{\text{Fe}_2(\text{SO}_4)_3}, m_{\text{NH}_3}, \dot{m}_{in,\text{Feed}}, \dot{m}_{in,\text{H}_2\text{SO}_4}, \dot{m}_{in,\text{Fe}}) \quad 4.2$$

The rates of impurities removal, such as arsenic and lead, were not included as part of the ML exercise because they are rapidly removed from solution to below their detection limits in the first autoclave compartment – that is, they were assigned arbitrary fast rate constants:



During normal plant operation, the compartmental samples are only analysed for FA – that is, to control the addition of weak aqua retrospectively. With the above micro-model framework in place, it became clear that calibration data was needed to better understand the chemical system. Doubt was also created by the variety of different shades of red to brown colours observed in the final autoclave residue (after the filter presses). Furthermore, the residue composition from the normal operational analyses, shown in Figure 3, gave no mechanistic insight into the processes occurring in the autoclave. All these factors prompted a short dedicated sampling campaign.

SAMPLING CAMPAIGN

General

The transient model was fully developed by the time the sampling campaign planning started. In fact, the DT, albeit not yet trained, pinpointed where the knowledge gaps were and how to best leverage the available plant resources to generate this additional information. The campaign ran over the last week of August 2023 and only utilised existing plant operators and laboratory staff.

The first set of analyses were used to confirm whether any iron(II) remained in the autoclave after the first compartment (A1). The iron(II) was below its detection limit, which signified that the A1 block analyses were ideal for regressing the DT micro model. This is because the feed flow and composition were fully defined, while the chemistry was not dominated by slow iron(II) oxidation.

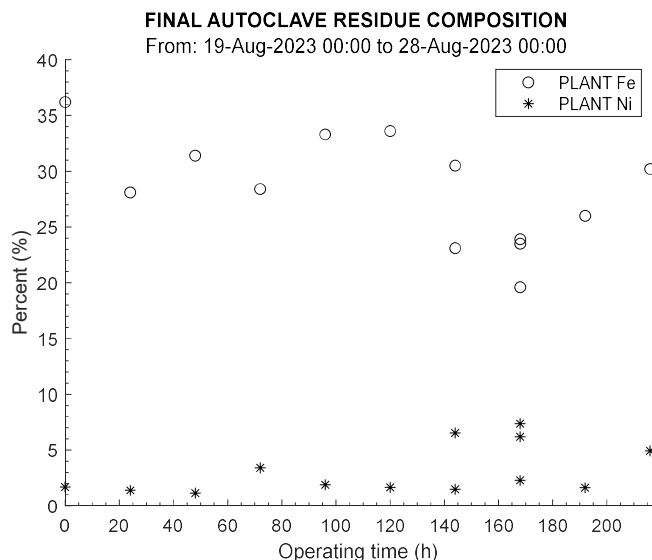


Figure 3: Final residue composition (after filter presses) from normal operational analyses.

Figure 3 shows that nickel was present in varying quantities in the final residue (dropped from the filter presses). At that stage, it was not understood whether the nickel was the remnant of incomplete washing cycles or co-precipitation. The residue samples from the Autoclave A compartments (A1, A2, A3) and Autoclave B compartments (B1, B2, B3) were therefore dried (without washing) in an oven at slightly elevated temperatures and analysed. Figure 4 shows photos of selected A3 residues on different sampling-campaign days. The wide range of different compartment residues were subsequently submitted for X-ray Diffraction (XRD) analyses to help shed some light on the precipitation chemistry.

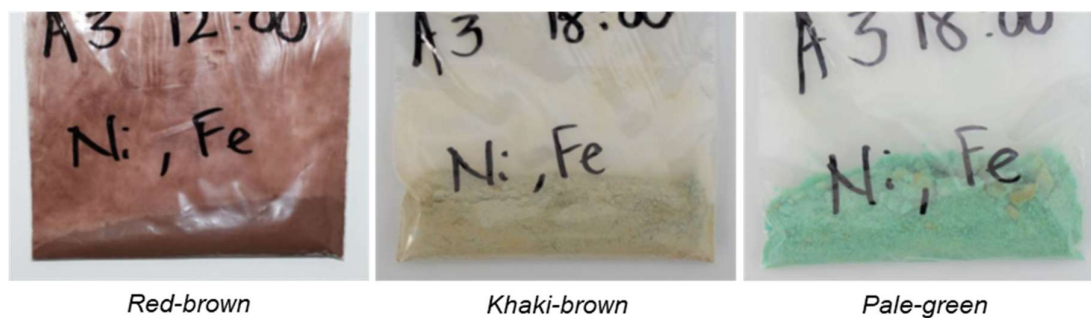


Figure 4: Selected compartment A3 residues on different sampling-campaign days.

The XRD results were definitive (Figure 5) – the major crystalline phase identified in the brown and red-brown samples was ammonium jarosite, $\text{NH}_4\text{Fe}_3(\text{SO}_4)_2(\text{OH})_6$. The khaki-brown and pale-green samples contained increasing to dominant amounts of ammonium nickel sulfate hexahydrate, $(\text{NH}_4)_2\text{Ni}(\text{SO}_4)_2 \cdot 6\text{H}_2\text{O}$, respectively. Nickel sulfate hexahydrate, $\text{NiSO}_4 \cdot 6\text{H}_2\text{O}$, was also present in minor quantities, but assumed to be a remnant of drying the unwashed residues.

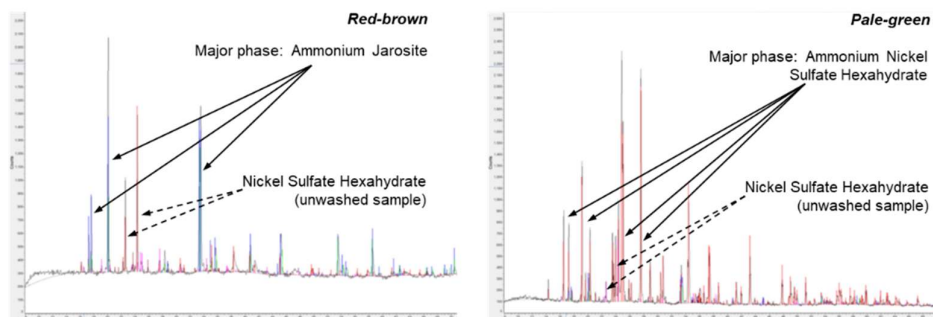
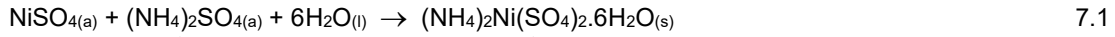


Figure 5: XRD results used to identify the major crystalline phases.

These results prompted the following expansion of the micro model:



$$\dot{m}_{r,x,7} = k_7 = f(\dot{m}_{\text{NH}_3}, \dot{m}_{\text{in,Feed}}, \dot{m}_{\text{in,H}_2\text{SO}_4}, \dot{m}_{\text{in,NH}}) \quad 7.2$$

Model training

The campaign data was loaded into the model workspace and then used to train the ML algorithms associated with the various reaction rates in A1. The first ML block was set up to vary the neutralisation rate k_2 (Equation 2.2) to mimic the measured FA concentration. Weighting vectors were used to adjust the weak aqua flowrates to each compartment, based on how many valves opened simultaneously at any specific point in time. Figure 6 summarises the outputs of this initial algorithm training exercise.

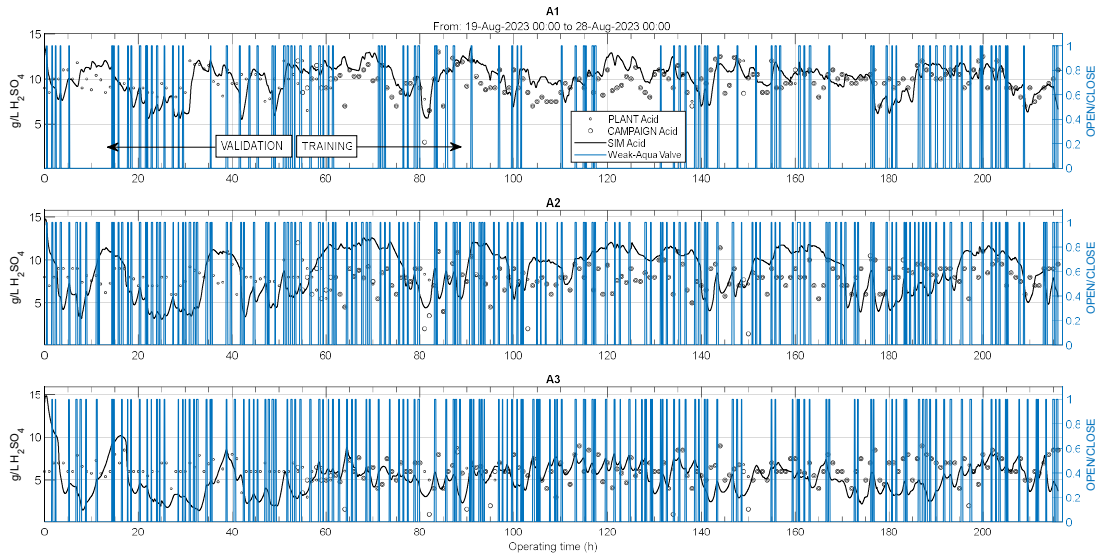


Figure 6: Outputs of the trained ML algorithms used to mimic the FA concentration in A1.

The simulated FA behaviour in the downstream compartments A2 and A3 could be improved in the future by also including those blocks in the training phase, as well as measuring the actual weak aqua flows. It is noteworthy that the system is highly transient due to the infrequent on/off pulses of weak aqua to the various compartments. Figure 7 shows an excerpt of the FA behaviour over a narrower time span – it demonstrates the transient responses to the weak aqua pulses and also serves to put the behavioural model accuracy in context with the typical measurement error.

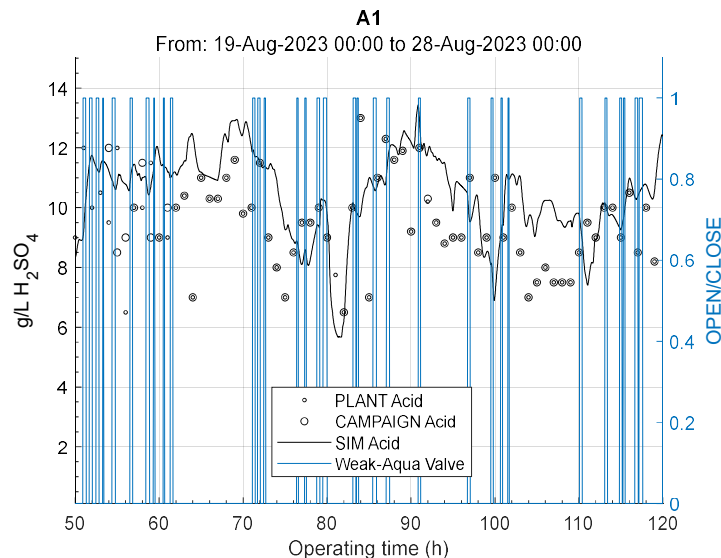


Figure 7: Example of the mimicked FA behaviour in A1 over a narrower time span.

The total oxidation rate k_3 , via the two parallel pathways (Equations 3.2 & 3.4), was trained so that the iron(II) concentration fell to below its detection limit in A1 – that is, as confirmed by measurement during the sampling campaign. The fraction of the precipitated iron present as the hydrated hematite (goethite) phase x_{Fe} was trained to match the measured iron content in the A1 residue. Coincidentally, this fraction naturally converged to small values (dominant jarosite phase).

The ammonium jarosite precipitation rate k_4 (Equation 4.2) was trained to match the iron(III) concentration remaining in the A1 solution. Figure 8 shows the first-round training output.

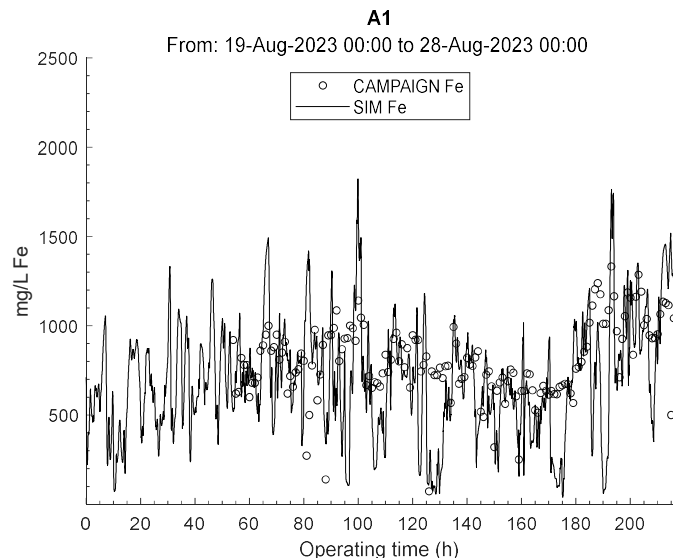


Figure 8: Output of the trained ML algorithms used to mimic the Fe concentration in A1.

The final ML exercise focused on matching the solids phase nickel content in the A1 compartment – that is, training the nickel precipitation rate k_7 (Equation 7.2) via the formation of ammonium nickel sulfate hexahydrate salt. The contribution of nickel sulfate hexahydrate salt, from drying unwashed residues during the campaign analyses, was assumed to be negligible.

SIMULATION RESULTS

Model validation

The ML blocks, trained on the campaign data for A1, were embedded in the hybrid DT model. The DT model was then used to simulate the iron behaviour in A2 and A3 – this is shown in Figure 9.

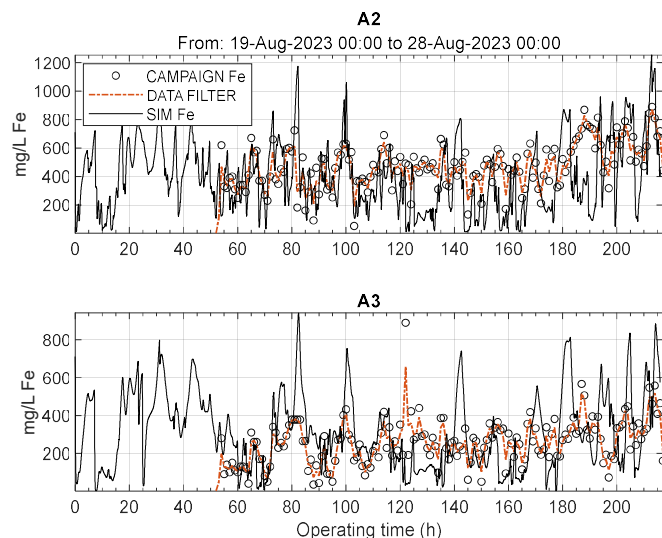


Figure 9: Model validation of the solution Fe concentration in A2 & A3.

Since the campaign data for A2 and A3 were previously unseen by the model, this served as validation of the simulated behaviour. Figure 10 compares the Autoclave A residue compositions to the corresponding model predictions for all three compartments. The FP part of the hybrid DT provides structure to the model and this, in turn, creates a sound generalisation methodology that often surpasses measurement accuracy. The model also corroborates the sampling campaign XRD results, suggesting that ammonium jarosite is the dominant iron-containing phase.

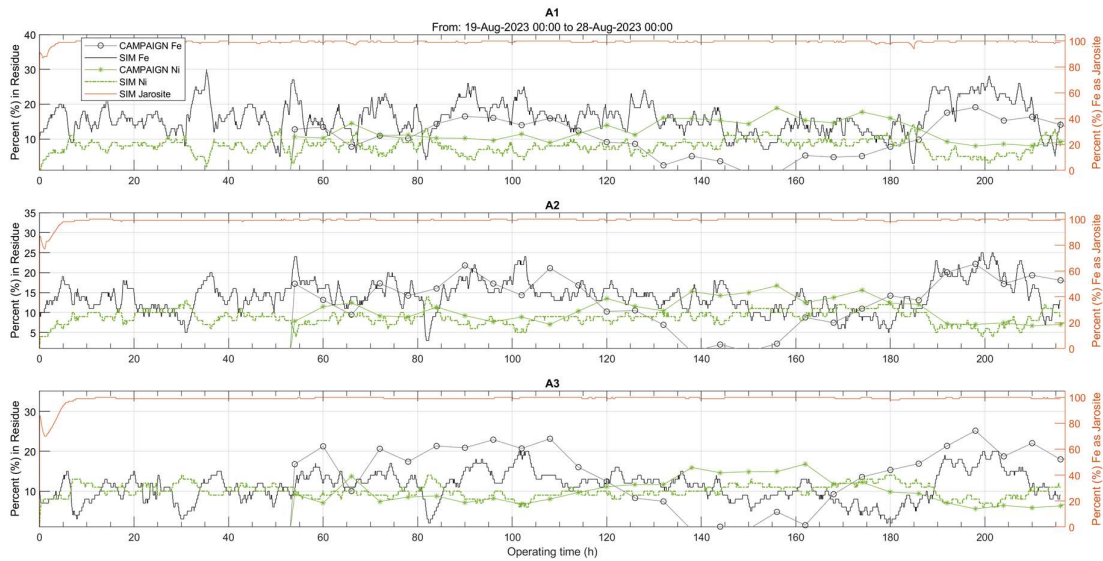


Figure 10: Model validation of the Autoclave A residue composition.

Insights

With the first-round training and validation completed, the DT was used to help explain day-to-day plant issues and observations, and to help make predictions on how the operation could potentially be improved in the future.

Figure 11 repeats the washed filter-press residue data (from the normal operational analyses for the 2nd half of the campaign run) presented in Figure 3, but also superimposes the simulated autoclave residue composition in A3 (albeit not washed). The simulated autoclave residue composition gives insight into the seemingly arbitrary spikes in the final residue nickel content (and the corresponding drops in the iron content) obtained from the plant measurements. Periods of excessive ammonium nickel sulfate hexahydrate salt formation in the autoclave showed up as higher nickel (> 5% Ni) and lower iron (< 25% Fe) in the final residue, likely due to inefficient washing in the filter presses.

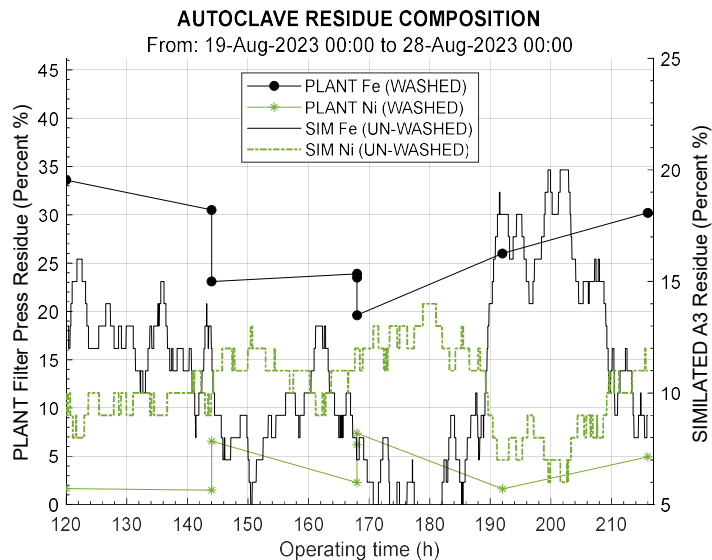


Figure 11: Final residue composition after washing (filter presses) vs the simulated A3 residue composition before washing.

The DT was used to help identify possible reasons behind the observed salt precipitation behaviour. One parameter that featured prominently during training of the rate k_7 (Equation 7.2), and which improved the model performance, is the autoclave feed flowrate, $\dot{m}_{in,Feed}$. Figure 12(a) plots this feed flowrate data, and its moving median. This suggests that prolonged periods of lower feed rates, e.g., between 140-160 h, and hence longer autoclave residence times, could promote ammonium nickel sulfate hexahydrate salt precipitation in the autoclave. A digital experiment was therefore conducted to simulate stabilising the feed flowrate by recycling filtrate back to the feed tank. Figure 12(b) shows the A2 aqua valve position, and its Gaussian-weighted moving average. It shows that longer autoclave residence times naturally result in lower weak-aqua flows since the operators set the weak-aqua valve timers based on the FA analyses. Nevertheless, the weak-aqua dosage rates could still have been too high, e.g., between 160-180 h.

In the next digital experiment, the DT was used to predict the outcome if the weak aqua flow to each compartment was varied proportionally to the autoclave feed flowrate and modulated, instead of using on/off valves. Figures 13(a) and 13(b) compare the baseline (on/off), and the scaled modulated cases, respectively. The benefit of the latter case is clearly demonstrated by the lower residue nickel content and the less erratic solution iron predictions. This result suggests that the feed flowrate of iron and acid should ideally be used to control the weak-aqua flows. There is therefore an opportunity to use the autoclave feed flowrate, the feed tank iron and acid tenors, and advanced process control (APC) algorithms to improve the operation. This DT model would be the ideal platform to develop and test such APC algorithms, without any risk to the actual plant operation. These optimised algorithms could then be gradually implemented on the plant for testing, with the ultimate objective of making the operation less reliant on operator interpretation.

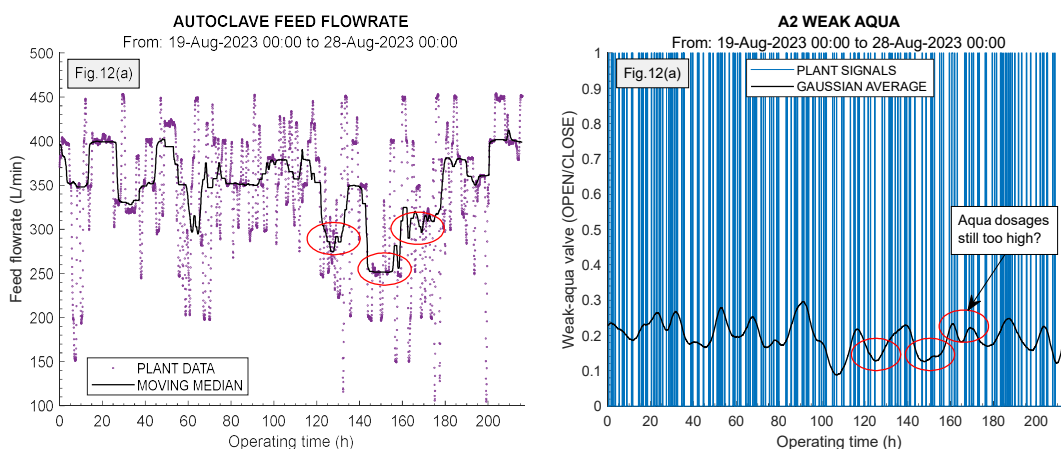


Figure 12: Variation of the (a) Autoclave feed flowrate, and, (b) A2 weak-aqua valve.

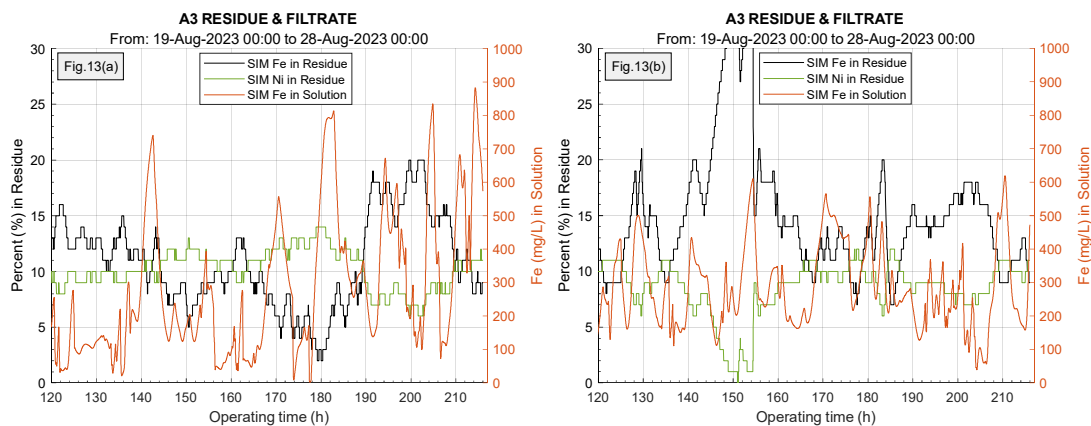


Figure 13: DT simulation of the (a) baseline, and, (b) scaled and modulated weak aqua flows.

Another noteworthy operational issue is the filtration rate through the filter presses. Since the feed pump to the filter presses is controlled by gap control, a persistent drop in the feed flowrate signifies filtration problems. Figure 14 compares the moving median of this flowrate with the simulated A3 pulp density (solids percent).

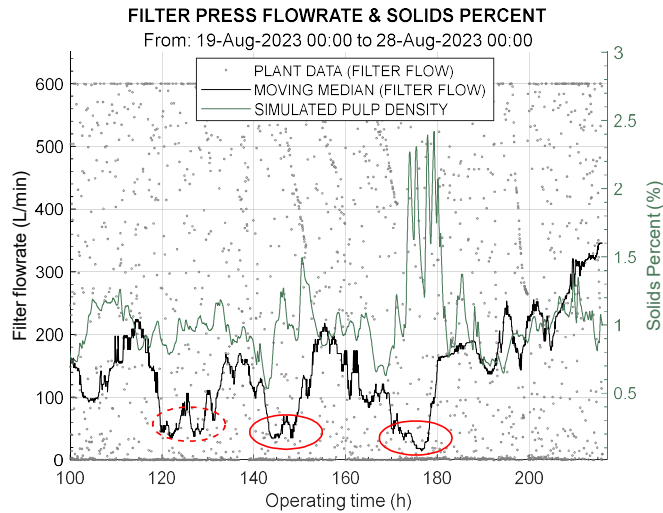


Figure 14: Measured filter feed flowrate vs the simulated A3 pulp density (solids percent). The encircled periods indicate persistent slower filtration rates on the plant.

Periods of slow filtration are encircled, while the predicted spikes in the simulated pulp density are due to the preferential precipitation of ammonium nickel sulfate hexahydrate salt. Despite some anomalies in Figure 14, these results suggest a correlation between the preferential formation of the ammonium nickel sulfate hexahydrate, predicted by the DT, and the slow filtration periods experienced on the plant. Furthermore, nickel losses would depend on the filterability and washing efficiency of the residue, and some of these slow filtration periods align with the elevated nickel levels in the final plant residue from the filter presses (Figure 3).

The above results and insights were gained from evaluating a single simulation period and utilising only an initial ML exercise. Importantly, the DT will be exposed to more datasets in the future and learning will improve – this is the real benefit of implementing a DT on an operational plant. To make the DT available to the operational staff, it has been packaged as an application product (APP) and distributed as a stand-alone executable.

CONCLUSIONS

The jarosite autoclaves at Implats have been in operation since the 1980's⁽⁵⁾. The plant works well, but relatively little new metallurgical information has been generated since its commissioning. Operational issues, like slow filtration, and perceptions of different precipitate phases forming, based on the colour of the final iron residue, have prompted a fresh look at the plant data. Since the operation is dominated by highly transient behaviour, modern state-of-the-art digital tools had to be utilised for this purpose. The results of developing and using a digital twin (DT) to capture the plant data, supplemented by data from a short sampling campaign, are discussed in this paper.

The backbone of the DT is the first-principles (FP) transient mass-energy balance (macro model), which is implemented in a manner that makes extensive use of machine learning (ML) to capture the complicated microscopic-level chemistry (micro model). The FP part of this hybrid DT provides structure to the model, which, in turn, helps to generalise and predict. Albeit exposed to only a single dataset, this powerful digital tool has been validated, and shown to be capable of predicting trends and creating insights into the low-level workings of the plant.

The hydrolysis of iron is driven by the injection of weak aqueous ammonia (aqua) by on/off valves to each autoclave compartment. The DT supports the sampling-campaign X-Ray Diffraction (XRD) analyses, suggesting that ammonium jarosite is the dominant iron hydrolysis product. Furthermore, the results have shown that the precipitation of ammonium nickel sulfate hexahydrate salt was most prominent during long autoclave residence time periods, when the weak-aqua dosage rates may have been too high. What-if scenarios were simulated, showing that valve modulation (instead of on/off timers) has potential. Advanced process control (APC) is also worth considering in the future.

The DT has been implemented as a standalone APP that can be exposed to more datasets in the future. It essentially becomes a 'living' digital report of the process to help improve operating strategies, process control, and operator training.

ACKNOWLEDGMENTS

The authors would like to thank the management of Implats for their vision, collaboration and permission to publish this paper. The authors are also grateful to Dauw Venter for providing the plant data, to Nagitta Kasirye for managing the sampling campaign, to Georg Langenhoven and Alida-Louise Henning for all the campaign analyses, and to Ian Smith for the XRD analyses.

The views of the authors do not necessarily represent those of Implats or its consultants.

REFERENCES

1. Steyl, J.D.T., Grobbelaar, G.B., 2020. Digital twinning in the metallurgical industry: the role of behavioural modelling and simulation. XXX International Mineral Processing Congress (IMPC) Proceedings, Cape Town, South Africa, 18-22 October 2020, 1-12.
2. The MathWorks Inc., Natick, MA, MATLAB, Simulink, Simscape, Release 2024a.
3. Dynamet, 2015. Dynamet Insights (Pty) Ltd., <https://dynamet.co.za>.
- 4.
5. OLI Systems Inc., Parsippany, NJ, OLI Studio, Stream Analyzer v11.5.
6. Plasket, R.P., Dunn, G.M., 1986. Iron rejection and impurity removal from nickel leach liquor at Impala Platinum Limited. International Symposium on Iron control in Hydrometallurgy Proceedings, Toronto, Canada, 19-22 October 1986, Ch. 37, 695-718.